Computational Materials Science 150 (2018) 369–380

Contents lists available at ScienceDirect

Computational Materials Science

journal homepage: www.elsevier.com/locate/commatsci

Heat and fluid flow in additive manufacturing – Part II: Powder bed fusion of stainless steel, and titanium, nickel and aluminum base alloys

T. Mukherjee[a], H.L. Wei[a], A. De[b], T. DebRoy[a,*]

[a] Department of Materials Science and Engineering, The Pennsylvania State University, University Park, PA 16802, USA
[b] Department of Mechanical Engineering, Indian Institute of Technology, Bombay 400076, India

ARTICLE INFO

Keywords:
Powder bed fusion
Additive manufacturing
Heat and fluid flow
Lack of fusion defect
Distortion

ABSTRACT

The most important metallurgical variables that affect the structure and properties of components produced by powder bed fusion (PBF) are examined using a model, proposed and validated in part-I of this paper. These variables include the temperature and velocity fields, build shape and size, cooling rates, solidification parameters, dendrite arm spacing, hardness, distortion and lack of fusion defects for four common alloys used in additive manufacturing (AM), stainless steel 316 (SS 316), Ti-6Al-4V, Inconel 718 and AlSi10Mg. The process parameters examined include laser power, scanning speed, powder layer thickness, packing efficiency and hatch spacing. Among the four alloys, the largest molten pool of AlSi10Mg ensures good fusional bonding among layers and hatches but exhibits high solidification shrinkage. Therefore, AlSi10Mg is the most susceptible to distortion among the four alloys. SS 316 exhibits the opposite trend because of its smallest molten pool among the four alloys. For a particular alloy, lack of fusion and distortion can be minimized by careful selection of hatch spacing and scanning speed. For the dendritic growth of SS 316 and AlSi10Mg, refinement of the solidification microstructure through close spacing of the dendrite arms can be achieved using thinner layers and faster scanning. Asymmetry in liquid pool geometry because of the difference in the thermal properties of powder bed and solidified build can be minimized by reducing the scanning speed.

1. Introduction

In laser-assisted powder bed fusion (PBF), alloy powders are added progressively in thin layers and melted using a laser beam. After solidification, the molten alloy takes the shape and size of the desired component [1]. Several complex physical processes take place during PBF. Absorption of the laser beam by the powder bed, melting of a region below the beam and its solidification occur rapidly. Inside the liquid pool, the metal circulates at fairly high velocities driven by the spatial gradient of surface tension and buoyancy force. Heat transfer affects the temperature field, local cooling rates, build shape and size and the extent of fusion between adjacent layers and hatches [1]. The complexity of the thermal cycles in a multi-layer, multi-hatch, component results in spatial variation of the microstructure and anisotropy of mechanical properties of the component. Rapid heating, cooling and solidification of the molten pool also make the components susceptible to distortion [1–3]. All these features must be taken into account for improved understanding of the laser assisted PBF process.

Several attempts have been made to model the heat transfer and fluid flow in PBF-AM process. Finite element based heat conduction models [4–9] are used to calculate 3D transient temperature distribution [4,5,8,9], build geometry [5,8], cooling rate, cell spacing, solidification morphology [4,5,8] and surface roughness [7]. However, these models ignore the effect of convective transport of heat inside the molten pool which is the main mechanism of heat transfer within the molten pool [1]. Therefore, the calculated temperature values and cooling rates are significantly overestimated [1]. In some investigations, the effects of liquid metal flow have been considered to calculate temperature distribution [10], build geometry [10–12], solidification morphology [10,13], microstructure evolution [14] and surface defects [15]. However, these calculations are often done for a single track [10–14] and unable to explain the causes of anisotropy and spatial non-uniformity of structure and properties observed in multi-layer, multi-hatch, builds. Thermo-physical properties are often assumed to be independent of temperature, powder size and packing efficiency [15] for simplicity. Powder scale models [16–22] consider convective flow of molten metal and properties that depend on temperature, powder size and packing efficiency and are applicable for multi-layer, multi-hatch, components. They are used to predict residual stresses [16], build geometry [16–19], lack of fusion defects [20–22] and spatter formation

* Corresponding author.
E-mail address: debroy@psu.edu (T. DebRoy).

https://doi.org/10.1016/j.commatsci.2018.04.027
Received 17 February 2018; Received in revised form 10 April 2018; Accepted 11 April 2018

[22]. However, they are often applied in 2D [19] and are computationally intensive [16,17]. Two-dimensional models are not suitable for calculating important metallurgical variables such as, cooling rates, solidification parameters and grain structure. Transport phenomena based mathematical frameworks provide an improved understanding of PBF process. What is needed and currently not available is a rigorously tested and computationally efficient numerical framework that considers the effects of molten metal convection and accurate thermo-physical properties of powder bed. Such models can calculate the most important metallurgical variables such as the fusion zone geometry, temperature and velocity fields, cooling rates and solidification parameters for multi-layer, multi-hatch builds for various AM variables.

In part I of this paper, a 3D transient heat transfer and fluid flow model of PBF-AM was developed and tested. The model solves the equations of conservation of mass, momentum and energy to calculate temperature and velocity fields, build shape and size and cooling rates from the process parameters and alloy properties. The model considers the convective flow of liquid metal inside the molten pool that is often the main mechanism of heat transfer within the liquid pool. The model also takes into account temperature dependent powder bed properties calculated based on powder particle size and packing efficiency. A travelling grid system is used to enhance the computational efficiency for multi-layer, multi-hatch calculations. Here the model is applied to calculate temperature and velocity fields, fusion zone shape and size, cooling rates, solidification parameters, arm spacing of columnar dendrites, micro-hardness, susceptibility to lack of fusion defects and distortion. The calculations are done for multi-layer, multi-hatch builds of four commonly used alloys, stainless steel 316 (SS 316), Ti-6Al-4V, Inconel 718 (IN 718) and AlSi10Mg.

2. Results and discussions

Table 1 lists the properties of the powders [23] used in the calculations. The computational domain (in Fig. 1) consists of powder bed, substrate and 5 layers, 5 hatches, build. The X-, Y- and Z- directions represent the scanning, hatching and building directions, respectively. For simplicity, a unidirectional scanning strategy is considered where the laser beam travels along the positive X-direction for all layers and hatches. Process variables and dimensions of the computational domain used in calculations are provided in Table 2.

2.1. Temperature and velocity fields

Fig. 2 shows the computed temperature and velocity fields during the building of the first layer first hatch with four different alloy powders. The red colored region bounded by the liquidus temperature isotherm of an alloy represents the fusion zone of the molten pool. The green colored region within the liquidus and the solidus temperature isotherms represents the mushy zone. Since the laser beam travels in the direction of positive X-axis, the molten pool is elongated in the opposite direction (negative X-axis). The molten pool exhibits a teardrop shape that is attributed to rapid scanning speed commonly used in the PBF process. The computed velocity vectors within the molten pool are shown by black arrows. The magnitude of these velocity vectors can be found out by comparing their length with the reference vector provided. The velocity vectors are radially outward as molten metal flows in the direction of positive temperature gradient [22–27]. For a

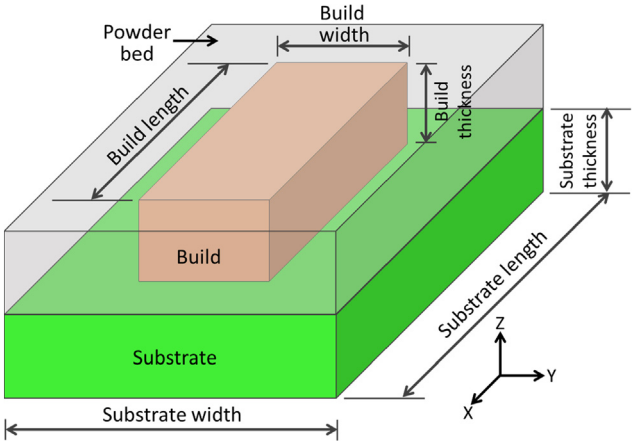

Fig. 1. Schematic of the solution domain consisting of substrate, powder bed and build. X, Y and Z directions represent the scanning, hatching and building directions, respectively.

Table 2
Process parameters used for calculations.

Parameter set	1	2
Laser power, W	60	110
Scanning speed, mm/s	250–1000	100
Spot radius, mm	0.05	0.30
Layer thickness, mm	0.025–0.035	0.30
Hatch spacing, mm	0.035–0.105	0.30
Build length, mm	20	5.28
Substrate dimensions, mm × mm × mm	22 × 5 × 2	7.17 × 4 × 1
Packing efficiency	0.5	0.4

Table 1
Thermo-physical properties of SS 316, Ti-6Al-4V, IN 718 and AlSi10Mg [23]. Here 'T' represents temperature in K ranging from ambient to the solidus temperature.

Properties	SS 316	Ti-6Al-4V	IN 718	AlSi10Mg
Liquidus temperature (K)	1733	1928	1609	867
Solidus temperature (K)	1693	1878	1533	831
Thermal conductivity (W/m K)	$11.82 + 1.06 \times 10^{-2}\,T$	$1.57 + 1.6 \times 10^{-2}\,T - 1 \times 10^{-6}\,T^2$	$0.56 + 2.9 \times 10^{-2}\,T - 7 \times 10^{-6}\,T^2$	$113 + 1.06 \times 10^{-5}\,T$
Specific heat (J/kg K)	$330.9 + 0.563\,T - 4.015 \times 10^{-4}\,T^2 + 9.465 \times 10^{-8}\,T^3$	$492.4 + 0.025\,T - 4.18 \times 10^{-6}\,T^2$	$360.4 + 0.026\,T - 4 \times 10^{-6}\,T^2$	$536.2 + 0.035\,T$
Density (kg/m^3)	7800	4000	8100	2670
Latent heat of fusion (J/kg)	272×10^3	284×10^3	209×10^3	423×10^3
Viscosity (kg/m s)	7×10^{-3}	4×10^{-3}	5×10^{-3}	1.3×10^{-3}
$d\gamma/dT$ (N/m K)	-0.40×10^{-3}	-0.26×10^{-3}	-0.37×10^{-3}	-0.35×10^{-3}
Absorption coefficient in liquid (η_l)	0.3	0.3	0.3	0.3
Absorption coefficient in powder (η_P)	0.7	0.7	0.7	0.7
Volumetric expansion coefficient (/K)	5.85×10^{-5}	2.5×10^{-5}	4.8×10^{-5}	2.4×10^{-5}
Young's modulus (GPa)	206	110	207	68